

Spin pumping and inverse spin Hall effect in CoFeB/IrMn heterostructures

Koustuv Roy,¹ Abhisek Mishra,¹ Pushpendra Gupta,¹ Shaktiranjana Mohanty,¹ Braj Bhusan Singh,¹ and Subhankar Bedanta^{1,2,*}

¹Laboratory for Nanomagnetism and Magnetic Materials (LNMM), School of Physical Sciences, National Institute of Science Education and Research (NISER), HBNI, Jatni-752050, India

²Center for Interdisciplinary Sciences (CIS), National Institute of Science Education and Research (NISER), HBNI, Jatni, 752050 India

The spin current based electronics, known as spintronics, is the promising technology to replace the charge current based technology. Spintronics based devices allow miniaturization of the device and faster response. The study of spin current efficiency in different materials is one of the emergent research topics in modern days. Spin pumping and inverse spin Hall effect (ISHE) are popular tools to study the spin to charge current conversion efficiency in the materials. In last one decade, ISHE and spin pumping are heavily investigated in ferromagnet (FM)/ heavy metal (HM) heterostructures. Recently the antiferromagnetic (AFM) materials are found to be a good replacement of heavy metals (HM) for these kind of studies. Faster dynamics, exhibiting very high spin-orbit coupling, absence of stray field, efficient propagation of spin current make AFM to be a good replacement of HMs. Understanding the role of different FM layers in a FM/AFM heterostructure for ISHE or spin pumping study is very important for spin to charge conversion physics. In this context we have performed the ISHE in CoFeB/ IrMn heterostructures. Spin pumping study is carried out for $Co_{60}Fe_{20}B_{20}(12nm)/Cu(3nm)/Ir_{50}Mn_{50}(tnm)/AlO_x(3nm)$ samples where t value varies from 0 to 10 nm. The Cu(3 nm) buffer layer is used which is less than the spin diffusion length(~ 8 nm) of Cu to improve the IrMn growth. The 3 nm Cu layer allows the unperturbed spin current propagation in the heterostructures. Damping of all the samples is higher than the single layer CoFeB which indicates that the spin pumping is due to the presence of IrMn. Further the spin pumping in the samples are confirmed by ISHE measurement. The real part of spin mixing conductance ($g_r^{\uparrow\downarrow}$) = $0.704 \pm 0.01 \times 10^{18} m^{-2}$ is found to be maximum in IrMn(2 nm) sample from the ISHE analysis. The large Spin Hall angle was also found to be ~ 0.30 for all the samples.

I. INTRODUCTION

Spin transport phenomena is one of the timely topics to develop the future spintronic devices[1, 2]. The generation and manipulation of the pure spin current is important for future technological devices and fundamental research as well. Production of pure spin current via spin pumping [3–7] is an efficient method which does not require nanofabrication in ferromagnetic (FM)/heavy metal (HM) systems. In this process the magnetization of FM is excited by a rf magnetic field through ferromagnetic resonance (FMR) and it generates the spin current (J_s) at the FM/HM interface, which is given by [2]:

$$\vec{J}_s = \frac{\hbar}{4\pi} g_r^{\uparrow\downarrow} \hat{m} \times \frac{d\hat{m}}{dt} \quad (1)$$

where $g_r^{\uparrow\downarrow}$ is the real part of spin mixing conductance and \hat{m} is the unit vector of magnetization. The procession under time varying field can generate resultant dc current which diffuses towards FM/HM interfaces. It can be converted into transverse charge current and hence transverse voltage can be measured by inverse spin Hall effect (ISHE). ISHE voltage is given by [8]:

$$V_{ISHE} \propto \theta_{SH} |\vec{J}_s \times \vec{\sigma}| \quad (2)$$

where θ_{SH} is the spin Hall angle which defines spin current to charge current conversion efficiency, and $\vec{\sigma}$ is the spin matrix governed by spin polarization direction. In order to get ISHE signal, θ_{SH} needs to be large in the heterostructure, which depends on the spin orbit interaction (SOI) of the HM. The spin to charge current conversion efficiency mostly depends on SOI of HM and its conductivity [2, 9].

Efficient and high spin current generation at low power with cost-effective materials at room temperature is still a challenge. Therefore, low damping FM materials (e.g. Py, CoFeB etc.) are very important to generate large spin pumping signal (ISHE voltage) by relatively suppressing the other spurious effects. Interface effect, impurity, magnetic proximity effects (MPE) etc., are the spurious effects which also enhance the value of damping constant. Further the selection of HM is very important for obtaining high ISHE. However there are only a few HMs in the periodic table and usually they are quite expensive. On the other hand recent works show antiferromagnets (AFM) exhibit high spin-orbit coupling and efficient transfer of spin angular momentum via antiferromagnetic spin waves [10–12]. Thus AFMs offer a good replacement for HMs as they also exhibit high SOI and there are many AFMs yet to be explored. Importantly FM/AFM bilayers have been heavily used in spintronics device application due to the exchange bias property [13]. In addition to that the ISHE study on this FM/AFM bilayers can give rise to new scope in spintronics for future device applications.

* sbedanta@niser.ac.in

The collinear AFM (i.e. Mn_2Au , IrMn etc.) is reportedly found to be exhibiting high θ_{SH} [10, 12, 14]. The collinear AFMs of CuAu-I type (e.g., IrMn, PtMn, FeMn, PdMn etc.) took great interest in this field for their simple crystal structure. Further they are easy to grow in the crystalline phase which is very much essential in spintronic device application purpose. IrMn exhibits high θ_{SH} within the CuAu-I AFMs. Most of the ISHE works on IrMn have been performed with crystalline FM materials like Py [15–17]. There are very few reports of spin pumping with CoFeB/IrMn bilayers [18–20]. The previous works lag systematic ISHE analysis. In this work, we have systematically studied the ISHE on the CoFeB/Cu/IrMn heterostructures. The crystallinity of the FM also plays a role in spin transport phenomena as it directly affects the interface of the FM/AFM. We have introduced a spacer Cu(3 nm) layer to improve the growth of IrMn further. The lower thickness of Cu layer in comparison to its spin diffusion length (~ 8 nm)[21] allows unperturbed spin current propagation from CoFeB to IrMn.

II. EXPERIMENTAL DETAILS

Table I shows the sample structure of our study. All the samples were prepared on Si(100) substrates using magnetron sputtering in a vacuum system with base pressure $\sim 5 \times 10^{-8}$ mbar. R1 and R2 are called the reference samples. The thickness of the films were evaluated using x-ray reflectivity (XRR) (data not shown) and transmission electron microscope(TEM) imaging. Crystalline quality of the thin films is also characterized by X-ray diffraction (XRD) and TEM imaging. The magnetic measurement was performed by superconducting quantum interference device (SQUID) based magnetometer.

Ferromagnetic resonance (FMR) measurements have been performed in the frequency range 5-16 GHz on a coplanar wave guide in the flip-chip manner [22, 23]. ISHE measurements have been performed by connecting a nanovoltmeter over two ends of the sample (sample size: 3 mm \times 2 mm). The details of the ISHE set-up can be found elsewhere [11, 12, 23–28].

III. RESULTS AND DISCUSSION

Crystalline quality

Grazing incidence X-ray diffraction(GIXRD) was performed on the S5 sample with X-ray of wave-length 0.15 nm. Fig. 1(a) shows the GIXRD pattern of the sample S6. We could clearly see the XRD peaks at 43.1° and 74° which correspond to IrMn(111) and Cu(220), respectively. The CoFeB has been grown in the amorphous form, therefore it does not show any XRD peaks.

The fig.1(b) shows the TEM image of S6 sample. It clearly shows the amorphous nature of the CoFeB and

TABLE I. Samples studied for the present work (The numbers in the bracket are in the units of nm).

R1	CoFeB(12)
R2	CoFeB(12)/Cu(3)
S1	CoFeB(12)/Cu(3)/AlO _x (3)
S2	CoFeB(12)/Cu(3)/IrMn(0.5)/AlO _x (3)
S3	CoFeB(12)/Cu(3)/IrMn(0.75)/AlO _x (3)
S4	CoFeB(12)/Cu(3)/IrMn(2)/AlO _x (3)
S5	CoFeB(12)/Cu(3)/IrMn(5)/AlO _x (3)
S6	CoFeB(12)/Cu(3)/IrMn(10)/AlO _x (3)

existence of crystallinity in IrMn. The Cu layer is not clearly visible in the image due to its low thickness value in our samples. The image also indicates the interdiffusion of Cu layer with its neighbouring layers. Further, we have performed line scan energy dispersive X-Ray analysis (EDX) of the sample as shown in fig.1 (c,d). The EDX result confirms the existence of all the elements in the sample structure in table I.

Magnetic Damping

In order to study the damping properties of the samples, the FMR measurement was carried out in the 5-16 GHz *rf* frequency range. Fig. 2(a) and (b) show the plots of resonance frequency (f) versus H_r and ΔH versus f , respectively. H_r and ΔH values were evaluated using FMR spectra. In order to evaluate the effective demagnetization ($4\pi M_{eff}$) and gyromagnetic ratio (γ), 2(a) was fitted to Kittel's equation [29] which is given as:

$$f = \frac{\gamma}{2\pi} \sqrt{(H_K + H_r)(H_K + H_r + 4\pi M_{eff})} \quad (3)$$

where

$$4\pi M_{eff} = 4\pi M_s + \frac{2K_s}{M_s t_{FM}} \quad (4)$$

and K_s , H_K , M_s , t_{FM} , are perpendicular surface magnetic anisotropy constant, anisotropy field, saturation magnetization and thickness of FM layer, respectively. The Gilbert damping(α) was evaluated by fitting data of Fig. 2(b) using the following expression [30]:

$$\Delta H = \Delta H_0 + \frac{4\pi\alpha f}{\gamma} \quad (5)$$

where, ΔH_0 is the inhomogeneous broadening of linewidth. α of a FM material depends upon the crystal structure as well as its band structure. In presence of any NM layer with HM, the interface plays a big role to modify the α . In such cases, the total α of the system can be written as:

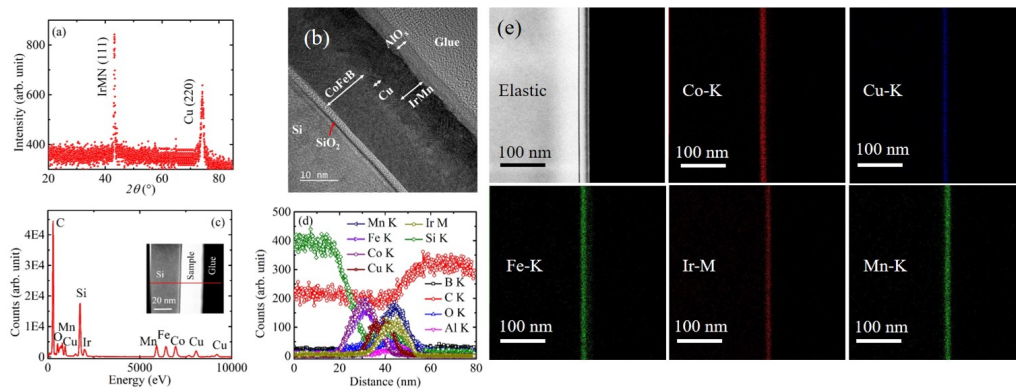


FIG. 1. (a) GIXRD pattern, (b) high resolution cross-sectional TEM image, (c) line scan EDX (inset image shows the selected area), (d) corresponding EDX scan profile of sample S6. (e) Elemental mapping using EFTEM for S6 at different energy edges.

$$\alpha = \alpha_{int} + \alpha_{impurity} + \alpha_{MPE} + \alpha_{sp} \quad (6)$$

where α_{int} is the intrinsic damping, and $\alpha_{impurity}$, α_{MPE} , and α_{sp} are the contribution from impurity, magnetic proximity effect (MPE) and spin pumping to the α , respectively [31].

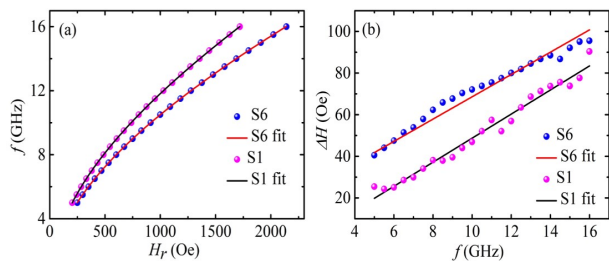


FIG. 2. (a) f vs H_r and (b) ΔH vs f plots for the samples S1 and S6. The solid lines are the best fits according to the equations 3 and 5.

The ΔH_0 value is larger for S6 (15 Oe) in comparison to S1 (1 Oe) which indicates a good homogeneity in the sample without the IrMn layer (S1). The almost linear behaviour of ΔH vs f rules out possibility of two magnon mechanism in our sample. The values of α for the S1-S6 are 0.0085, 0.0102, 0.0101, 0.0100, 0.0103, 0.0099 and R1-R2 are 0.0087, 0.0081 with the error bar ± 0.0001 respectively. Clearly one can see that the damping value enhances by significant margin in presence of IrMn layer. Reference sample's α values are almost similar in comparison to the sample S1. Thus, we may conclude that the damping enhancement in our samples are actually coming because of IrMn layer.

From fig 4, it is observed that the value of α for the sample S2 (IrMn=0.5 nm) is maximum. Beyond this IrMn thickness limit the α value is almost saturating. This behaviour can be explained with the spin diffusion length of IrMn (~ 0.7 nm) [10]. In case of dominant

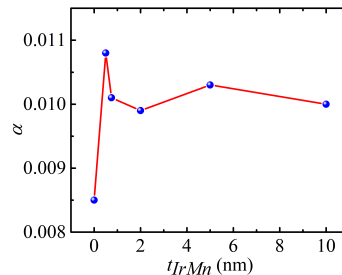


FIG. 3. α variation as a function of IrMn thickness (S1-S6).

spin pumping behaviour over the other interface effects, the α value saturates at the NM thickness equals to its spin diffusion length. However, we can not rule out the possibility of other interfacial effects like MPE on the total α value. In order to investigate the magnetic dead layer formation or MPE at the interface, we performed magnetization measurement on all the samples. The saturation magnetization (M_s) of all the samples are found to be 840.13 emu/cc (S1), 827.03 emu/cc (S2), 884.28 emu/cc (S3), 882.36 emu/cc (S4), 840.11 emu/cc (S5) and 849.97 emu/cc (S6). No significant change in the M_s value was observed. Thus we conclude that the dominant spin pumping behaviour in our samples.

Inverse spin Hall effect measurement

Damping analysis indicates the presence of spin pumping mechanism in the samples. In order to confirm the spin pumping and qualitative analysis of the spin current generation in our system, we performed ISHE measurements on all the samples. The measurements are carried out at 7 GHz frequency and +15 dBm r_f magnetic field power.

The measured electrical voltage in ISHE measurement has different contributions other than the spin pumping,

TABLE II. Fitted parameters from ϕ dependent voltage measurements for the samples with different IrMn thickness(S2-S6)

Sample	$V_{sp}(\text{V}) \times 10^{-6}$	$V_{AHE}(\text{V}) \times 10^{-6}$	$V_{AMR}^{\perp}(\text{V}) \times 10^{-6}$	$V_{AMR}^{\parallel}(\text{V}) \times 10^{-6}$
S2	1.14 ± 0.03	-0.43 ± 0.01	0.86 ± 0.01	0.14 ± 0.02
S3	1.49 ± 0.04	-0.74 ± 0.02	1.00 ± 0.01	0.23 ± 0.05
S4	1.47 ± 0.04	-0.75 ± 0.02	0.94 ± 0.02	0.33 ± 0.02
S5	1.21 ± 0.02	-0.18 ± 0.03	0.67 ± 0.01	0.10 ± 0.02
S6	1.24 ± 0.04	-0.65 ± 0.02	0.81 ± 0.01	0.09 ± 0.02

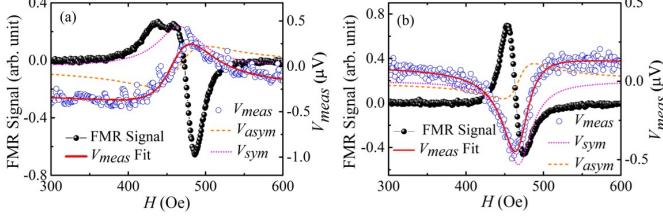


FIG. 4. Voltage (V_{meas}) measured across the sample with applied magnetic field along with FMR signal for sample S6 at the ϕ values of (a) 0° , (b) 180° . Experimental data is represented as open symbol. Solid lines are the fit to the experimental data using Eq. (7). Short dotted and dash lines are the symmetric (V_{sym}) and anti-symmetric (V_{asym}) components of the voltage.

e.g. anisotropic magnetoresistance (AMR) and anomalous Hall effect (AHE). Angle dependent voltage measurement have been performed to rectify these spurious effects. Fig. 4 shows the measured voltage (V_{meas}) (open blue symbol) versus H along with FMR signal (close black symbol) for sample S6 at the angles $\phi = 0^\circ$ (a) and 180° (b). The ϕ denotes the angle between the perpendicular direction of applied DC magnetic field (H) and measured voltage direction. It should be noted that the pumped spin current is invariant upon the sample rotation in the measurement. Upon the change in polarity of the voltmeter electrodes, the measured voltage should change sign in case of spin pumping in the samples. We found that the measured voltage (V_{meas}) is changing sign with the 180° rotation of the sample which is a clear indication of the presence of spin pumping in the sample. If the sign does not reverse with the 180° rotation of the sample, the measured voltage solely comes from the spurious effects other than the spin pumping. It should also be noted that the V_{meas} goes to zero value when the $\phi \sim 90^\circ$. According to the basic mechanism of electron spin scattering in ISHE, it happens because the spin accumulation is almost zero when the measured voltage direction is parallel to applied magnetic field. The maximum spin accumulation happens in the perpendicular direction to the applied magnetic field. In order to, quantify spin pumping contribution from the V_{meas} , the V_{meas} versus H plots for the samples S6 (Fig. 4) was fitted with Lorentzian equation[32], which is given by:

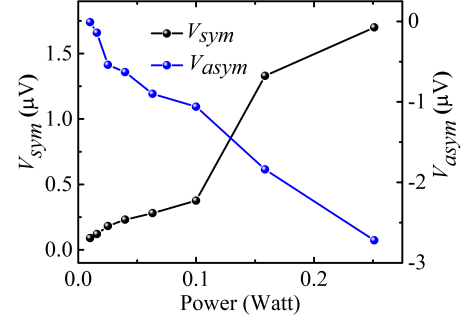


FIG. 5. V_{sym} and V_{asym} contribution with the variation of rf magnetic field power for the sample S6.

$$V_{meas} = V_{sym} \frac{(\Delta H)^2}{(H - H_r)^2 + (\Delta H)^2} + V_{asym} \frac{2\Delta H(H - H_r)}{(H - H_r)^2 + (\Delta H)^2} \quad (7)$$

where V_{sym} and V_{asym} are the symmetric and anti-symmetric Lorentzian components of the measured signal. Solid red lines are fits to the experimental data. The V_{sym} consists of major contribution from spin pumping, while minor contributions are from AMR, and AHE effects. Whereas the AMR and AHE are the major contributions in the V_{asym} component. Fig. 4 also represents the plot of V_{sym} (dotted line) and V_{asym} (dashed line) separately for the samples S6.

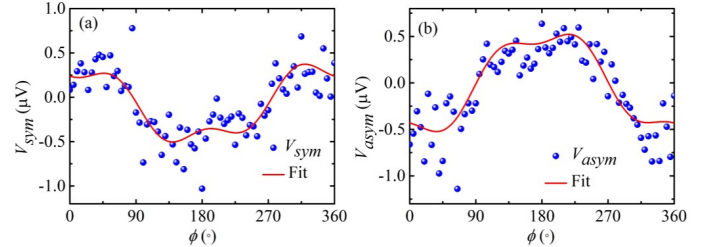


FIG. 6. Angle dependent (a) (ϕ) V_{sym} and (b) V_{asym} measurements for samples S6.

In order to quantify the spin pumping and other rectification contributions, In-plane angle dependent ISHE

measurements of V_{meas} were performed at the interval of 5° for all the samples (fig.6 shows for S6). This method is an established one to decouple the individual components from the measured voltage [31, 33, 34]. Harder *et.al.* [35] has considered the rectification effects i.e., the AHE contribution due to the FM layer, perpendicular AMR ($V_{asym/sym}^{AMR\perp}$) and parallel AMR ($V_{asym/sym}^{AMR\parallel}$) to the applied *rf* field. The relation between these rectification effects and V_{meas} are as follows [33]:

$$\begin{aligned} V_{asym} &= V_{AHE} \sin(\Phi) \cos(\phi + \phi_0) + \\ &V_{asym}^{AMR\perp} \cos 2(\phi + \phi_0) \cos(\phi + \phi_0) + \\ &V_{asym}^{AMR\parallel} \sin 2(\phi + \phi_0) \cos(\phi + \phi_0) \end{aligned} \quad (8)$$

$$\begin{aligned} V_{sym} &= V_{sp} \cos^3(\phi + \phi_0) + V_{AHE} \cos(\Phi) \cos(\phi + \phi_0) \\ &+ V_{sym}^{AMR\perp} \cos 2(\phi + \phi_0) \cos(\phi + \phi_0) \\ &+ V_{sym}^{AMR\parallel} \sin 2(\phi + \phi_0) \cos(\phi + \phi_0) \end{aligned} \quad (9)$$

V_{sp} and V_{AHE} correspond to the spin pumping and AHE contributions, respectively. Φ is the angle between *rf* field and applied DC magnetic field which is 90° for our set up. Thus, the AHE does not contribute to the V_{sym} term. The extra factor ϕ_0 takes care of the misalignment of sample positioning in defining the ϕ value during the measurement. Thus the equation 8 and 9 can be simplified as follows:

$$\begin{aligned} V_{asym} &= V_{AHE} \cos(\phi + \phi_0) + \\ &V_{asym}^{AMR\perp} \cos 2(\phi + \phi_0) \cos(\phi + \phi_0) + \\ &V_{asym}^{AMR\parallel} \sin 2(\phi + \phi_0) \cos(\phi + \phi_0) \end{aligned} \quad (10)$$

$$\begin{aligned} V_{sym} &= V_{sp} \cos^3(\phi + \phi_0) + \\ &+ V_{sym}^{AMR\perp} \cos 2(\phi + \phi_0) \cos(\phi + \phi_0) \\ &+ V_{sym}^{AMR\parallel} \sin 2(\phi + \phi_0) \cos(\phi + \phi_0) \end{aligned} \quad (11)$$

Further the total AMR contribution also can be quantified by the following formula [33]:

$$V_{AMR} = \sqrt{(V_{asym}^{AMR\perp, \parallel})^2 + (V_{sym}^{AMR\perp, \parallel})^2} \quad (12)$$

The $V_{asym}^{AMR\perp, \parallel}$ and $V_{sym}^{AMR\perp, \parallel}$ are evaluated from the in-plane angle dependent ISHE measurements by fitting V_{meas} values by equations 10 and 11, respectively. Similar angle dependent ISHE measurement was carried out for all the samples. The extracted various rectification components for all the samples are listed in the Table II. It should be noted that the samples without IrMn layer, S1, R1 and R2 do not show any ISHE signal (data not shown). It is expected as Cu does not have any high

SOC. This fact confirms that the spin pumping mechanism is occurring in the samples S2-S6 solely because of IrMn layer.

Table II clearly shows that the V_{sp} is dominating over other unwanted rectification effects in all the samples. However, the AHE contribution is not negligible in the samples. The AHE phenomena is controlled by the berry curvature[36] of the material. It is an intrinsic property of the FM layer. The Co based FM materials are always a potential candidate for the AHE contribution [37, 38]. The anisotropic nature of the samples can be understood from the finite contribution of AMR values. The positive values of V_{sp} indicates the positive spin Hall angle in IrMn, which is consistent with literature[10]. Fig. 5 shows the *rf* magnetic field power dependent V_{sym} and V_{asym} contribution for the sample S6. With the increase in power, the spin angular momentum transfer from FM to NM increases linearly. The linear behaviour in Fig. 5 is another signature of the spin pumping mechanism in sample S6.

The V_{sp} is found to be maximum for S3 which indicates the smooth interface between FM and NM. The spin pumping happens more at the thickness of NM which is equal to its spin diffusion length (λ). The λ_{IrMn} is previously reported to be 0.7 nm[10]. The high V_{sp} for S3 and S4 is consistent with this argument. The Eq. 17 shows that the V_{sp} depends upon the conductivity of the IrMn. At higher thickness of IrMn, the conductivity of IrMn increases. This leads to decrease in V_{sp} value for S5 and S6. In addition to this, the back spin pumping also dominates beyond the spin diffusion length of HM due to the spin flip mechanism at this thickness limit. Thus the decrease in V_{sp} value for S5 and S6 is possibly a cumulative contribution of conductivity as well as the spin back flow.

Effective spin mixing conductance ($g_{eff}^{\uparrow\downarrow}$) is another parameter which defines the efficiency of spin current propagation from FM to NM. Figure 7 shows the graph between $g_{eff}^{\uparrow\downarrow}$ and IrMn thickness. $g_{eff}^{\uparrow\downarrow}$ was calculated by the following expression using damping constant[2]:

$$g_{eff}^{\uparrow\downarrow} = \frac{\Delta\alpha 4\pi M_s t_{CoFeB}}{g\mu_B} \quad (13)$$

where $\Delta\alpha$, t_{CoFeB} , μ_B , g are the change in the α due to spin pumping, the thickness of CoFeB layer, Bohr magneton, Lande g- factor, respectively. The real part of $g_{eff}^{\uparrow\downarrow}$ mainly contributes to the spin transport mechanism. Thus, it is very crucial to quantify the real part of spin mixing conductance $g_r^{\uparrow\downarrow}$. The $g_r^{\uparrow\downarrow}$ value can be evaluated by the following expression[39, 40]:

$$g_r^{\uparrow\downarrow} = g_{eff}^{\uparrow\downarrow} \left[1 + \frac{g_{eff}^{\uparrow\downarrow} \rho_{IrMn} \lambda_{IrMn} e^2}{2\pi\hbar \tanh\left[\frac{t_{IrMn}}{\lambda_{IrMn}}\right]} \right]^{-1} \quad (14)$$

Where ρ_{IrMn} , λ_{IrMn} are the resistivity and spin diffusion length of IrMn respectively. In order to calculate

$g_r^{\uparrow\downarrow}$, the λ_{IrMn} is taken to be 0.7 nm [10]. The $g_r^{\uparrow\downarrow}$ values for S2-S6 found to be 0.606, 0.690, 0.704, 0.696, 0.687 nm^{-2} . It is also to be noted that our $g_r^{\uparrow\downarrow}$ values are one order less than the previously reported values with IrMn [10, 17, 20, 41]. The relatively lower value of $g_r^{\uparrow\downarrow}$ confirms that the spin current flow efficiency is not so good in our heterostructures. It is probably because Cu is not a good spacer layer for such heterostructures. This result supports our TEM image where Cu layer has been seen to be interdiffused with the neighbouring layers. Spin interface transparency (T) is the parameter which defines the spin current propagation efficiency at the FM/NM interface. T value is calculated from the following expressions[42]:

$$T = \frac{g_r^{\uparrow\downarrow} \tanh\left(\frac{t_{IrMn}}{2\lambda_{IrMn}}\right)}{g_r^{\uparrow\downarrow} \coth\left(\frac{t_{IrMn}}{\lambda_{IrMn}}\right) + \frac{\hbar\sigma_{IrMn}}{2e^2\lambda_{IrMn}}} \quad (15)$$

where σ_{IrMn} is the conductivity of IrMn layer. The maximum $g_r^{\uparrow\downarrow}$ is found to be in sample S4. For S4 ($t_{IrMn}=2$ nm), T is evaluated to be 0.14 ± 0.01 by Eq.15, which is much lower than the values reported in the literature for Pt based systems [42]. θ_{SH} is also another parameter which is very much important in spintronic device applications. We evaluated the θ_{SH} for the IrMn using the following expression [39, 40, 43]:

$$|\vec{J}_s| \approx \left(\frac{g_r^{\uparrow\downarrow}\hbar}{8\pi}\right)\left(\frac{\mu_0 h_{rf}\gamma}{\alpha}\right)^2 \times \left[\frac{\mu_0 M_s \gamma + \sqrt{(\mu_0 M_s \gamma)^2 + 16(\pi f)^2}}{(\mu_0 M_s \gamma)^2 + 16(\pi f)^2}\right] \left(\frac{2e}{\hbar}\right) \quad (16)$$

$$V_{sp} = \left(\frac{w_y}{\sigma_{FM}t_{FM} + \sigma_{NM}t_{NM}}\right) \times \theta_{SH} \lambda_{NM} \tanh\left(\frac{t_{NM}}{2\lambda_{NM}}\right) |\vec{J}_s| \quad (17)$$

The four probe technique was used to measure the resistivity (ρ) of the samples. The ρ_{IrMn} and ρ_{CoFeB} are found to be $5.5 \times 10^{-6} \Omega.m$ and $8.5 \times 10^{-6} \Omega.m$ respectively. σ corresponds to the conductivity of the individual layers.

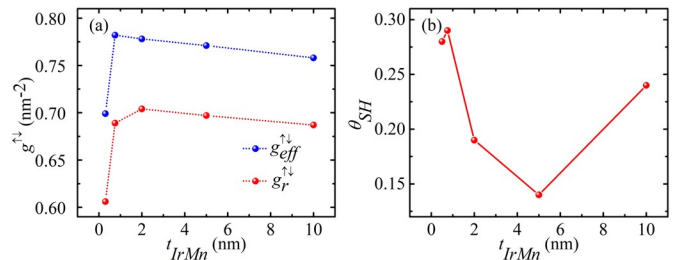


FIG. 7. (a) $g_{eff}^{\uparrow\downarrow}$, $g_r^{\uparrow\downarrow}$ and (b) θ_{SH} with the variation of IrMn thickness. Short dotted line in (a) is the guide to the eye.

The rf field ($\mu_0 h_{rf}$) and CPW transmission line width (w_y) value for our set up are 0.05 mT (at +15 dBm rf power) and 200 μm , respectively. Fig 7 shows the variation of θ_{SH} for the sample S2-S6. The highest $\theta_{SH}=0.30$ value is obtained for S3. This is higher than any other reported values for IrMn and also comparable with the Pt[10, 17].

IV. CONCLUSION

We presented the spin pumping and inverse spin Hall effect study in a series of CoFeB/ IrMn heterostructures. The IrMn has been grown in AFM phase. Angle dependent study was performed to disentangle all the spin rectification effects. Strong spin pumping contribution is found in the samples. The spin pumping voltage saturates at the spin diffusion length of the IrMn thickness. V_{sp} value decreases for higher value of IrMn thickness due to increase in conductivity of IrMn. The maximum $g_r^{\uparrow\downarrow}$ is evaluated to be $0.704 \times 10^{18} m^{-2}$ for S4. Spin transparency also found to be 0.14 which indicates that Cu is not a good spacer layer for IrMn and CoFeB. But, the high spin Hall angle of 0.30 in S3 predicts IrMn as a good replacement of HM in spintronic device applications.

ACKNOWLEDGEMENT

The authors acknowledge DAE and DST, Govt. of India, for the financial support for the experimental facilities. KR and PG thank CSIR and UGC for their JRF fellowships, respectively. BBS acknowledges DST for INSPIRE faculty fellowship. The authors thank Dr. T. Ghosh for help in TEM measurement.

REFERENCES

- [1] S. Bader and S. Parkin, Annu. Rev. Condens. Matter Phys. **1**, 71 (2010).
 [2] Y. Tserkovnyak, A. Brataas, G. E. Bauer, and B. I. Halperin, Reviews of Modern Physics **77**, 1375 (2005).

- [3] J. R. Sánchez, L. Vila, G. Desfonds, S. Gambarelli, J. Attané, J. De Teresa, C. Magén, and A. Fert, *Nature communications* **4**, 1 (2013).
- [4] X. Tao, Q. Liu, B. Miao, R. Yu, Z. Feng, L. Sun, B. You, J. Du, K. Chen, S. Zhang, et al., *Science advances* **4**, eaat1670 (2018).
- [5] B. Heinrich, C. Burrowes, E. Montoya, B. Kardasz, E. Girt, Y.-Y. Song, Y. Sun, and M. Wu, *Physical review letters* **107**, 066604 (2011).
- [6] M. Obstbaum, M. Decker, A. Greitner, M. Haertinger, T. Meier, M. Kronseder, K. Chadova, S. Wimmer, D. Ködderitzsch, H. Ebert, et al., *Physical review letters* **117**, 167204 (2016).
- [7] K. Chen and S. Zhang, *Physical review letters* **114**, 126602 (2015).
- [8] E. Saitoh, M. Ueda, H. Miyajima, and G. Tatara, *Applied physics letters* **88**, 182509 (2006).
- [9] Y. Tserkovnyak, A. Brataas, and G. E. Bauer, *Physical review letters* **88**, 117601 (2002).
- [10] W. Zhang, M. B. Jungfleisch, W. Jiang, J. E. Pearson, A. Hoffmann, F. Freimuth, and Y. Mokrousov, *Physical review letters* **113**, 196602 (2014).
- [11] B. B. Singh, K. Roy, J. A. Chelvane, and S. Bedanta, *Physical Review B* **102**, 174444 (2020).
- [12] B. B. Singh and S. Bedanta, *Physical Review Applied* **13**, 044020 (2020).
- [13] J. Nogués and I. K. Schuller, *Journal of Magnetism and Magnetic Materials* **192**, 203 (1999).
- [14] J. Zhou, X. Wang, Y. Liu, J. Yu, H. Fu, L. Liu, S. Chen, J. Deng, W. Lin, X. Shu, et al., *Science advances* **5**, eaau6696 (2019).
- [15] R. Hao, R. Zang, T. Zhou, S. Kang, S. Yan, G. Liu, G. Han, S. Yu, and L. Mei, *Chinese Physics B* **28**, 037202 (2019).
- [16] H. Wu, C. Wan, Z. Yuan, X. Zhang, J. Jiang, Q. Zhang, Z. Wen, and X. Han, *Physical Review B* **92**, 054404 (2015).
- [17] L. Frangou, S. Oyarzun, S. Auffret, L. Vila, S. Gambarelli, and V. Baltz, *Physical review letters* **116**, 077203 (2016).
- [18] D. Jhahria, D. K. Pandya, and S. Chaudhary, *Beilstein Journal of Nanotechnology* **9**, 2198 (2018).
- [19] S. Tu, J. Hu, G. Yu, H. Yu, C. Liu, F. Heimbach, X. Wang, J. Zhang, Y. Zhang, A. Hamzić, et al., *Applied Physics Letters* **111**, 222401 (2017).
- [20] X. Ma, G. Yu, S. A. Razavi, L. Chang, L. Deng, Z. Chu, C. He, K. L. Wang, and X. Li, *Physical Review B* **98**, 104428 (2018).
- [21] F. Jedema, M. Nijboer, A. Filip, and B. Van Wees, *Physical Review B* **67**, 085319 (2003).
- [22] “Nanosc ab,” .
- [23] B. B. Singh, S. K. Jena, and S. Bedanta, *Journal of Physics D: Applied Physics* **50**, 345001 (2017).
- [24] B. B. Singh, S. K. Jena, M. Samanta, K. Biswas, and S. Bedanta, *ACS Applied Materials & Interfaces* **12**, 53409 (2020).
- [25] B. B. Singh, K. Roy, P. gupta, Pushpendra, T. Seki, K. Takanashi, and B. Bedanta, *NPG Asia Mater* **13**, 11 (2021).
- [26] P. Gupta, B. Singh, K. Roy, A. Sarkar, M. Waschke, T. Brueckel, and S. Bedanta, *Nanoscale* (2021).
- [27] B. Sahoo, K. Roy, P. Gupta, B. Satpati, B. B. Singh, and S. Bedanta, *arXiv e-prints*, arXiv (2020).
- [28] B. B. Singh, S. K. Jena, M. Samanta, K. Biswas, B. Satpati, and S. Bedanta, *physica status solidi (RRL)–Rapid Research Letters* **13**, 1800492 (2019).
- [29] C. Kittel, *Physical review* **73**, 155 (1948).
- [30] B. Heinrich, J. Cochran, and R. Hasegawa, *Journal of Applied Physics* **57**, 3690 (1985).
- [31] A. Conca, S. Keller, L. Mihalceanu, T. Kehagias, G. Dimitrakopoulos, B. Hillebrands, and E. T. Papaioannou, *Physical Review B* **93**, 134405 (2016).
- [32] R. Iguchi and E. Saitoh, *Journal of the Physical Society of Japan* **86**, 011003 (2017).
- [33] A. Conca, B. Heinz, M. Schweizer, S. Keller, E. T. Papaioannou, and B. Hillebrands, *Physical Review B* **95**, 174426 (2017).
- [34] M. Harder, Y. Gui, and C.-M. Hu, *Physics Reports* **661**, 1 (2016).
- [35] M. Harder, Z. Cao, Y. Gui, X. Fan, and C.-M. Hu, *Physical Review B* **84**, 054423 (2011).
- [36] N. Nagaosa, J. Sinova, S. Onoda, A. H. MacDonald, and N. P. Ong, *Reviews of modern physics* **82**, 1539 (2010).
- [37] W. Zhang, V. Vlaminck, J. E. Pearson, R. Divan, S. D. Bader, and A. Hoffmann, *Applied physics letters* **103**, 242414 (2013).
- [38] G. Zahnd, L. Vila, V. Pham, M. Cosset-Cheneau, W. Lim, A. Brenac, P. Laczkowski, A. Marty, and J. Attané, *Physical Review B* **98**, 174414 (2018).
- [39] K.-R. Jeon, C. Ciccarelli, H. Kurebayashi, J. Wunderlich, L. F. Cohen, S. Komori, J. W. Robinson, and M. G. Blamire, *Physical Review Applied* **10**, 014029 (2018).
- [40] K. Rogdakis, A. Sud, M. Amado, C. Lee, L. McKenzie-Sell, K. Jeon, M. Cubukcu, M. Blamire, J. Robinson, L. Cohen, et al., *Physical Review Materials* **3**, 014406 (2019).
- [41] J. Holanda, H. Saglam, V. Karakas, Z. Zang, Y. Li, R. Divan, Y. Liu, O. Ozatay, V. Novosad, J. E. Pearson, et al., *Physical review letters* **124**, 087204 (2020).
- [42] W. Zhang, W. Han, X. Jiang, S.-H. Yang, and S. S. Parkin, *Nature Physics* **11**, 496 (2015).
- [43] K. Ando, S. Takahashi, J. Ieda, Y. Kajiwara, H. Nakayama, T. Yoshino, K. Harii, Y. Fujikawa, M. Matsuo, S. Maekawa, et al., *Journal of applied physics* **109**, 103913 (2011).